J. Fluid Mech. (2006), *vol.* 569, *pp.* 321–330.
doi:10.1017/S002211200600303X Printed in the United Kingdom

Flow-driven opening of a valvular leaflet

By G. PEDRIZZETTI[1] AND F. DOMENICHINI[2]

[1]Dipartimento Ingegneria Civile e Ambientale, Università di Trieste, P.le Europa 1, 34127 Trieste, Italy
[2]Dipartimento Ingegneria Civile, Università di Firenze, Via S. Marta 3, 50139 Firenze, Italy

(Received 7 March 2006 and in revised form 16 September 2006)

The understanding of valvular opening is a central issue in cardiac flows, whose analysis is often prohibited by the unavailability of (*in vivo*) data about tissue properties. Asymptotic or approximate representations of fluid–structure interaction are thus sought. The dynamics of an accelerated stream, in a two-dimensional channel initially closed by a rigid inertialess movable leaflet, is studied as a simple model problem aimed at demonstrating the main phenomena contributing to the fluid–structure interaction. The problem is solved by the coupled numerical solution of equations for the flow and solid. The results show that the leaflet initially opens in a no-shedding regime, driven by fluid mass conservation and a predictable dynamics. Then the leaflet motion jumps, after the saturation of a very rapid intermediate vortex-shedding phase, to the asymptotic slower regime with a stable self-similar wake structure.

1. Introduction

The interaction between a fluid stream and a moving boundary is common in several contexts; numerous examples can be found in the cardiovascular system where flows inside deformable vessels and through cardiac valves are of primary physiological relevance. The original motivation for this work is our interest in the flow through the mitral valve that controls the blood motion from the left atrium to the left ventricle of the heart. More generally, similar phenomena can be found in technological devices when valves are used to control the fluid motion through orifices and possibly to avoid back-flow. Despite the applied background this work is a theoretical one, on the interaction of the flow and a leaflet under ideal conditions. It represents a step towards the understanding of phenomena in a fluid-structure interaction of potentially high applied relevance.

When a closed valve is forced to open by a stream, the (typically thin) leaflets rapidly move with the fluid with only a weak resistance to it. A rigorous mathematical model of the flow–structure dynamics should be based on the fluid and solid equations, for the flow and the tissue, respectively, and on the proper coupling relations. Along these lines, a simplified approach, developed for a thin solid without bending stiffness, was introduced by Peskin & McQueen (1989). However, in our experience, the numerical implementation of this mathematically attractive model has several disadvantages, such as the lack of resolution close to the body and unrealistic stress distributions on it. A major difficulty in studying the fluid–solid interaction is the rapidity of the leaflet response to the action of the incoming fluid, and its large movement within the flow domain. A complete numerical solution of the fluid-solid system has been presented for the flow in models of the aortic valve (De Hart *et al.* 2003; Stijnen *et al.*

2004). These remarkable studies introduced an accurate coupling strategy within a finite element solution method.

In addition to these difficulties, the development of a well-posed mathematical model must account for large deformations, in the nonlinear regime, of the valvular visco-elastic solid elements. However, little is known about the material parameters of biological elements like cardiac valve leaflets, principally because such quantities are not accessible *in vivo*. They are typically non-homogeneous and non-isotropic, differing between individual people and in a single person with aging. A homogeneous and isotropic Neo-Hookian elastic approximation for the aortic valve was employed in De Hart *et al.* (2003), and a linearly elastic leaflet in Stijnen *et al.* (2004). In general, the valve behaviour and its parameters are unknown and difficult to assess in physiological applications (Stevens *et al.* 2003). Therefore, the realistic reproduction of the fluid dynamics in the presence of biological leaflets still appears an ambitious objective.

It has been noted that the interaction between valves and accelerating flows is modified in specific cardiovascular diseases (Handke *et al.* 2003, for example, and references therein) but, despite the potential implications of the topic, little is known about the mechanics involved. Some studies have focused on the fluid dynamics only, avoiding a detailed description of the solid properties using *ad hoc* boundary conditions (Baccani, Domenichini & Pedrizzetti 2003), or assuming a held-open mitral valve when studying left ventricular fluid dynamics (Lemmon & Yoganathan 2000; Domenichini, Pedrizzetti & Baccani 2005). Some progress has been achieved with lumped-parameter models (Szabo *et al.* 2004, and references therein) that are aimed at reproducing specific measurements, based on a number of model parameters, and are not intended to explain the corresponding vorticity dynamics. A different approach, to overcome the difficulties found when describing the solid properties, was considered by Pedrizzetti (2005) with a derivation of the leaflet motion based on fluid dynamical concepts only. That work showed that, in the limiting case of vanishing viscosity, the assumption of absence of shedding from the leaflet trailing edge (Kutta condition) leads to a characteristic relation between the leaflet angular velocity and the velocity of the incoming stream, which applies well to the viscous case also. However, the dynamical meaning of such an assumption remained unknown.

The aim of this work is to contribute to the understanding of the flow-driven opening of valvular leaflets when material parameters are not readily accessible. This study, although originated from a physiological interest, is a theoretical one and aims to uncover general behaviours in an ideal system. It considers the interaction between the flow in a two-dimensional channel and a leaflet that is rigid and inertialess, when the valve opening is driven by the fluid only without additional viscoelastic resistance. This is a basic model, simple enough to be analysed thoroughly, that contains the main general features, or their asymptotic limit, of many transvalvular flows. On the other side, such a simple model does not contain features like the flexible structure of the leaflet or the three-dimensionality, which could play fundamental roles.

2. Mathematical formulation

Consider the viscous flow in a two-dimensional rectilinear channel with half-width H, due to an accelerating discharge whose section-averaged velocity starts from zero at time zero and reaches a peak value V_p at time T. The channel is initially closed by the leaflet, which then opens with the flow. Taking H and V_p as scales for length and velocity, respectively, the dimensionless problem is characterized by the peak

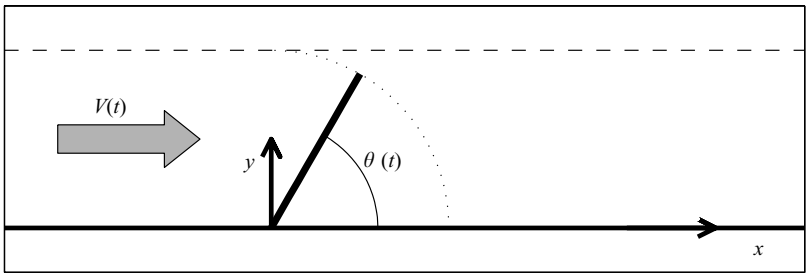

FIGURE 1. Sketch of the physical problem.

Reynolds number $Re = V_p H/\nu$, where ν is the kinematic viscosity, and the Strouhal number $St = H/V_p T$. For convenience, the dimensionless time is further normalized by multiplication with St, so that the time-law of the dimensionless discharge $V(t)$ has $V(1) = 1$.

The fluid dynamics is governed by the two-dimensional Navier–Stokes and continuity equations written in the vorticity–streamfunction (ω, ψ) formulation (Roache 1998)

$$St\frac{\partial \omega}{\partial t} + \frac{\partial \psi}{\partial y}\frac{\partial \omega}{\partial x} - \frac{\partial \psi}{\partial x}\frac{\partial \omega}{\partial y} = \frac{1}{Re}\nabla^2\omega, \tag{2.1}$$

$$\nabla^2\psi = -\omega. \tag{2.2}$$

A rectilinear leaflet of infinitesimal thickness and of unitary (dimensionless) length is hinged on the lower wall, corresponding to the origin of the system of coordinates (x, y) that describes the flow domain, figure 1. The leaflet can rotate clockwise, its motion being specified by the angle $\theta(t)$, so that when $\theta = \pi/2$ the channel is completely closed, and when $\theta = 0$ the plate lies on the lower channel wall. The system of equations (2.1), (2.2) is completed by the boundary conditions. At the wall $y = 0$ the no-slip conditions $v_x = v_y = 0$ are imposed and $\psi = 0$; the centreline $y = 1$ is a symmetry line where $\psi = V(t)$. At $x = \pm\infty$ uniform flows are assumed. On the moving leaflet, the no-slip condition gives $v_r = 0$ and $v_n = -rSt\dot{\theta}$, where v_r and v_n are the components of the velocity tangential and normal to the leaflet, respectively, r is the distance from the origin, and $\dot{\theta} = \mathrm{d}\theta/\mathrm{d}t$, on the leaflet $\psi = -St\dot{\theta}r^2/2$. The flow starts from rest at $t = 0$, when $\theta = \pi/2$.

The formulation still requires the definition of the dynamical equation for the solid. The leaflet is infinitely rigid and can rotate about the ideal hinge at $x = 0$ without any elastic or viscous resistance other than that due to the flow action. Therefore, the unique equation for the solid element is the balance of angular momentum, i.e. $\mathscr{T} = 0$, $\mathscr{T}$ being the torque acting on the body. Writing the Navier–Stokes equations in terms of primitive variables on the fore and rear faces of the leaflet, the tangential balance gives

$$\frac{\partial}{\partial r}(p_f(r,t) - p_r(r,t)) = \frac{1}{Re}\left(\left.\frac{\partial \omega}{\partial n}\right|_f - \left.\frac{\partial \omega}{\partial n}\right|_r\right), \tag{2.3}$$

where the subscripts r and f stand for rear and fore, respectively, and the torque $\mathscr{T}$ acting on the valve is

$$\mathscr{T} = \int_0^1 (p_f(r,t) - p_r(r,t))r\,\mathrm{d}r = -\frac{1}{Re}\int_0^1 r\,\mathrm{d}r\int_r^1 \left(\left.\frac{\partial \omega}{\partial n}\right|_f - \left.\frac{\partial \omega}{\partial n}\right|_r\right)\mathrm{d}s. \tag{2.4}$$

After replacing the integrals in (2.4) using the equality between $\int_0^1 f(s)\int_s^1 g(r)\,\mathrm{d}r\,\mathrm{d}s$ and $\int_0^1 g(s)\int_0^s f(r)\,\mathrm{d}r\,\mathrm{d}s$, the leaflet zero-torque equation is finally rewritten as

$$\mathscr{T} = -\frac{1}{2Re}\int_0^1 \left(\left.\frac{\partial\omega}{\partial n}\right|_f - \left.\frac{\partial\omega}{\partial n}\right|_r \right) r^2\,\mathrm{d}r = 0. \tag{2.5}$$

Equation (2.5) must be solved with (2.1), (2.2) to specify the motion of the solid element.

3. Numerical method

The problem defined in § 2 has been solved numerically. Equations (2.1), (2.2) are made discrete on a regular Cartesian grid with standard second-order centred finite differences. The moving leaflet is accounted for using a (ω, ψ) version of the immersed boundary method (Fadlun *et al.* 2000; Pedrizzetti 2005), where the grid points near the plate are handled with particular care. At each time step, a variable numbers of fictitious points are added, corresponding to the intersection of the leaflet with the computational grid, say $(x_b(r_b, t), y_b(r_b, t)) = (r_b\cos\theta(t), r_b\sin\theta(t))$. At these points, the streamfunction and its derivatives are known, that is $\psi_b = -St\dot{\theta}r_b^2/2$, $\partial\psi/\partial r|_b = -St\dot{\theta}r_b$, and $\partial\psi/\partial n|_b = 0$. Whereas the streamfunction is continuous across the leaflet, the vorticity field is discontinuous and different values for the fore and rear faces, ω_{bf} and ω_{br}, are considered.

During the advancement of (2.1), the vorticity values at the leaflet are used to evolve the value of ω at the points of the computational grid next to the valve in order to avoid the computation of any derivatives across the leaflet. Once vorticity ω has been updated at the inner points of the domain using (2.1), the streamfunction ψ is computed solving the discrete version of (2.2), a linear system, and forcing the known boundary conditions. At the same time, (2.5) is used to compute the leaflet motion as an additional linear equation in (2.2) including the additional unknown $\dot{\theta}$, as follows: The discretization of the normal derivative in (2.5) gives a linear combination of the vorticity values at the wall and inside the flow field. When solving (2.2), the values of vorticity inside the integration domain are known and thus enter as known terms; however, the wall vorticity is expressed in terms of ψ close to and at the wall, the latter being proportional to $\dot{\theta}$. Thus (2.5) can be recast in terms of known values of ω, unknown values of ψ, and the additional unknown $\dot{\theta}$, similarly to what has been done in different contexts (Pedrizzetti & Domenichini 1997; Pedrizzetti 1998). The value of $\dot{\theta}$ is then used to advance in time the leaflet position together with (2.1) for the flow field. The vorticity at the leaflet surfaces is computed from the known streamfunction field: (2.2) is evaluated at the boundary using a formal Taylor expansion in the x- and y-directions to estimate the second derivatives at the wall, similarly to what is done at the $y = 0$ wall (Roache 1998).

The solution has been obtained with a domain of finite length in the x-direction at the boundary of which a zero second x-derivative condition is imposed on both ω and ψ. Typically, the computational domain extends from $x = -1$ to $x = 6$; tests have been made to ensure that the flow near the valve and the valvular motion are independent of the domain extent. The number of grid points in the y-direction has been set to $N_y = 128$ and the same grid spacing has been used in the x-direction. The sensitivity to the resolution has been checked varying N_y from 32 to 192; the solution is shown to converge for $N_y \geqslant 96$. The results shown here are thus evaluated with a grid of 896×128. The time advancement is performed with a second-order

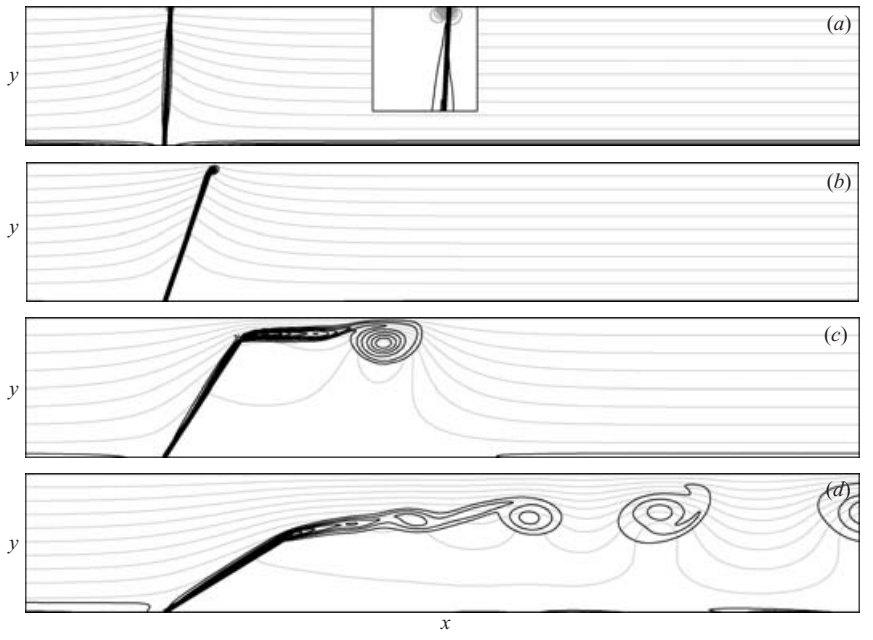

FIGURE 2. Streamlines and vorticity field, $St = 0.1$, $Re = 10^3$; (*a*) $t = 18/128$, (*b*) $t = 36/128$, (*c*) $t = 54/128$, (*d*) $t = 90/128$. Streamfunction values (light grey) are equally spaced between their minimum value and $V(t)$. Vorticity levels: (*a*) from -10 to 10, step 0.5; (*b–d*) from -100 to 100, step 5. Black and grey lines (see enlarged view in (*a*)) correspond to negative and positive values, respectively.

Adams–Bashforth method and time step chosen to satisfy the convective and viscous stability criteria (Roache 1998).

4. Results

The problem is first studied at $Re = 1000$ and $St = 0.1$ using the temporal law $V(t) = (1 - \cos(\pi t))/2$. Then, the temporal law $V(t)$ and parameters are varied to show how the results are influenced by them. These reference values have been selected to be representative of a normal mitral flow (remember that the period T considered here is the accelerating phase of the early ventricular diastole that is about 1/10 of the heartbeat). This relatively small value for the Reynolds number is representative for children and is selected for consistency with the two-dimensional approximation. However, the analogy of this ideal model with actual cardiac flows should not be taken further.

In figure 2 the flow evolution is reported at different instants of time in terms of instantaneous streamlines and vorticity distribution. Initially, the valve opens quickly and the flow is mainly irrotational with weak boundary layers of negative (clockwise, corresponding to black lines in figure) vorticity that develop on both sides of the leaflet, see figure 2(*a*) at $t = 18/128$. No evident shedding is found and, instead, during the very initial phase some positive (counterclockwise, grey in figure 2*a* inset) vorticity close to the leaflet edge is seen. Then, the upstream boundary layer begins to separate from the trailing edge, figure 2(*b*) at $t = 36/128$, and then rolls up to form an attached vortex. The subsequent evolution is characterized by the growth of the shed vortex, which becomes the head of a vortex jet, figure 2(*c*) at $t = 54/128$. The fully developed

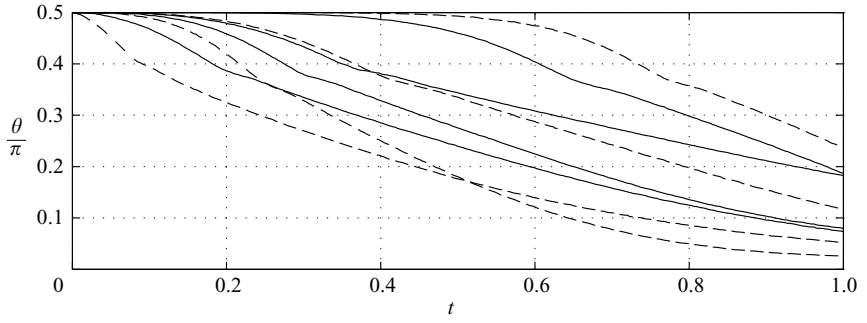

FIGURE 3. Time evolution of θ/π, $Re = 10^3$. From left to right at the top of the figure ($\theta \approx 0.4\pi$) cases 4, 5, 2, 1, 3, 6, 7, 8; odd cases are continuous lines, even are dashed.

wake takes the form of an elongated vortex sheet originating from the trailing edge, occasionally with the appearance of local Kelvin–Helmholtz roll-up, figure 2(*d*) at $t = 90/128$.

In order to show how the dynamics are influenced by the specific type of accelerating profile, the same simulation has been performed but halving and doubling the Strouhal number to $St = 0.05$ and $St = 0.2$, cases 2 and 3, respectively. Other solutions have then been considered by replacing $V(t)$ with power laws $t^{1/2}$, t, t^2, t^4, t^6, cases 4 to 8. The simulations have been performed to $t = 1$. In all the cases the evolution is qualitatively similar, although the timing of events varies with the flow acceleration. The leaflet dynamics are shown in figure 3 in terms of the time profiles $\theta(t)$. All the curves show an initial opening up to $\theta \approx 0.4\pi$, where a sudden change of the slope is noticeable. This corresponds to the roll-up, saturation, and detachment of the shed vortex that marks the transition to a slower opening, when the wakes take the shape of an elongated vortex sheet.

The simplicity of the model problem allows one to extract some similarity information from dimensional analysis arguments: the functional dependence of the instantaneous variation of the leaflet angle can be expressed in dimensional terms as

$$\frac{\mathrm{d}\theta}{\mathrm{d}t^*} = \mathscr{F}(\theta, H, V^*(t^*), \nu), \tag{4.1}$$

where the superscript $*$ indicates dimensional quantities. Using the instantaneous velocity $V^* = V_p V(t)$ as the appropriate scale for instantaneous variations, equation (4.1) is rewritten in our standard dimensionless terms as

$$St\,\frac{\dot{\theta}(t)}{V(t)} = \mathscr{F}(\theta, Re_t), \tag{4.2}$$

where $Re_t = V(t)Re$ is the instantaneous Reynolds number. The functional dependence (4.2) is analysed in figure 4 by plotting $St\dot{\theta}/V$ versus θ for the 8 cases with the same peak Reynolds number $Re = 1000$. The profiles show a common behaviour during the initial phase, $\theta \lesssim \pi/2$, that corresponds to the early leaflet opening. Then the curves separate during their rapid rise, the rapid deceleration that corresponds to the change of slope in $\theta(t)$, and converge again, at lower velocity, toward an approximately common behaviour asymtotic to $\dot{\theta}/V = 0$ when $\theta = 0$. The curves in figure 4 indicate a weak dependence on the instantaneous Reynolds number during the intermediate period of the evolution.

In general, the dynamics of the leaflet can be classified into three phases as follows. During the initial stage, when the channel is almost closed, $\theta \lesssim \pi/2$, the flow presents an almost absence of shedding from the leaflet, whose motion is dominated by the

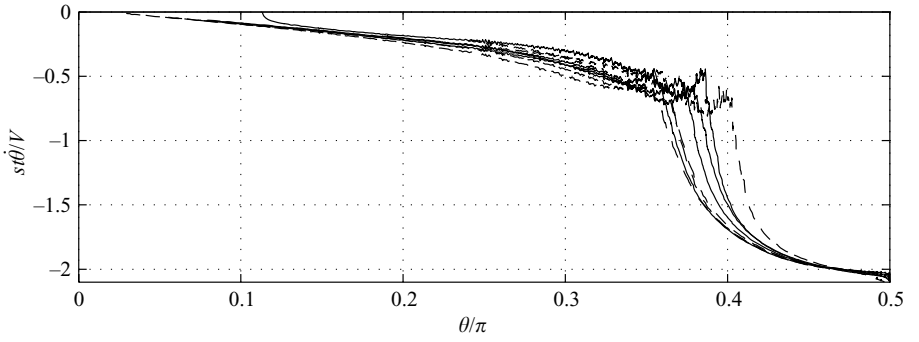

FIGURE 4. $St\dot{\theta}/V$ versus θ/π, $Re = 10^3$, all cases. Odd cases are continuous lines, even are dashed.

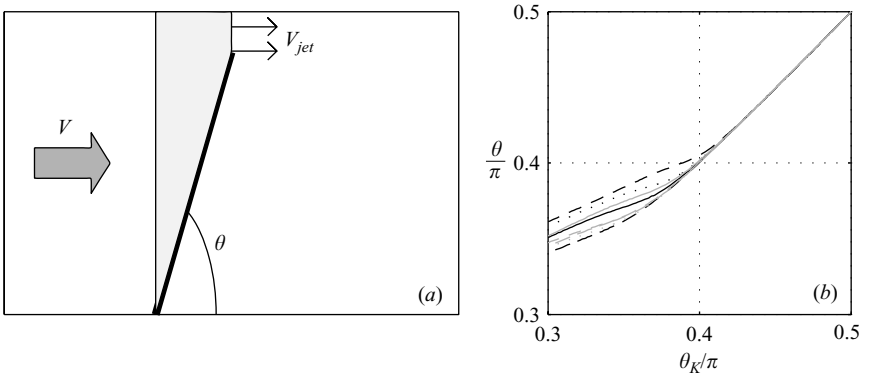

FIGURE 5. (*a*) Sketch of the mass balance (4.3). (*b*) Computed θ versus θ_K predicted with (4.4). Cases (1–4) black lines: continuous, dashed, dotted, dash-dotted, respectively. Cases (5–8) grey lines: continuous, dashed, dotted, dash-dotted, respectively.

mass balance. In this *no-shedding regime* the valve moves with the fluid to satisfy continuity, given the limited free opening above it. Mass conservation applied to the shadowed area in figure 5(*a*) can be written as

$$V_{jet}(1 - \sin\theta) - St\dot{\theta}/2 = V, \tag{4.3}$$

where V_{jet} is the average x-velocity of the jet exiting from the open part of the channel. The condition of no shedding corresponds to the absence of the component around the edge of the relative velocity between the flow and the leaflet. This condition can be written $V_{jet}\sin\theta = -St\dot{\theta}$, which represents an approximation of the Kutta condition using the average velocity V_{jet}; it was shown in Pedrizzetti (2005) that for $\theta \lesssim \pi/2$ this approximation does not differ significantly from the same condition evaluated with the local irrotational velocity. Insertion of this relation into the mass balance (4.3) gives

$$St\dot{\theta} = \frac{2V\sin\theta}{\sin\theta - 2}. \tag{4.4}$$

Formula (4.4) allows one to compute the initial time evolution of $\theta(t)$ with a straightforward time integration. In figure 5(*b*) we show the comparison between the computed $\theta(t)$ and $\theta_K(t)$ estimated with the Kutta condition (4.4), showing its good predictive capability until $\theta \approx 0.4\pi$.

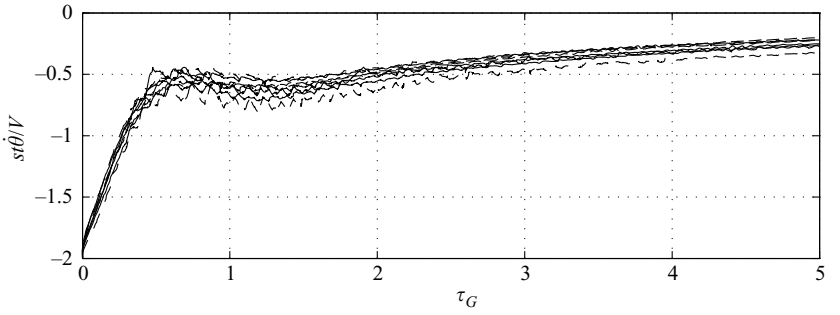

FIGURE 6. $St\dot{\theta}/V$ versus τ_G, $Re = 10^3$, all cases. Odd cases are continuous lines, even are dashed.

In the second phase of the evolution, the rigid leaflet offers resistance to the flow and induces vortex shedding from the trailing edge. During this *roll-up regime* the shed vorticity increases the pressure on the downstream side of the leaflet and decelerates its motion, giving rise to a well-developed vortex roll-up. The attached vortex moves faster than the leaflet edge and eventually detaches to become an elongated (multiple) vortex wake. This phenomenon is analogous to that studied in Gharib, Rambod & Shariff (1998) and Dabiri & Gharib (2005) in the different context of flows separating from a circular nozzle. They showed that the wake transition from an attached rolling-up leading vortex to a fully developed wake structure can be described by the critical value of a dimensionless parameter, which they call *formation time*. In the present context, the formation time is defined

$$\tau_G(t) = St^{-1} \int_{t_0}^{t} \Delta v(s)\, \mathrm{d}s, \tag{4.5}$$

where $\Delta v = V_{jet} + St\dot{\theta} \sin\theta$ is the relative velocity in the direction of vortex elongation; t_0 is the start time of the vortex formation, which means that the integral (4.5) is evaluated only during the period when $\Delta v > 0$. The behaviour of $St\dot{\theta}/V$ previously plotted in figure 4 is now replotted in figure 6 in terms of the formation time τ_G. All the curves now present a unique timing of the events in terms of the formation time. The scaled angular velocity of the leaflet has a maximum at $\tau_G \approx 0.7$. This corresponds to the instant when the leading vortex detaches from the edge, and it can be considered as the limiting value of τ_G that characterizes the transition from a single to multiple-vortex structure in the present context. Subsequently, the leaflet angular velocity is weakly reduced until reaching a following minimum, at $\tau_G \approx 1.4$, that precedes the final asymptotic decelerating profile.

The third and final phase of leaflet motion is characterized by the development of a fairly stable wake structure when the vortex has become the head of a vortex sheet leaving the trailing edge. During this *vortex-sheet regime* the flow below the sheet is almost stagnating (see figure 2*c*, *d*), with a pressure higher than in the jet zone, and the valve moves very slowly. The angular velocity of the leaflet $\dot{\theta}$ depends primarily on the stream velocity and on the position θ (see figure 4 for $\theta < 0.3\pi$) with a weak dependence on the Reynolds number. The functional relation (4.2) takes the asymptotic form

$$St\dot{\theta} = -V\kappa(Re) \left(\frac{\theta}{\pi}\right)^{\alpha(Re)}, \tag{4.6}$$

where $\alpha > 1$. The curve fitting values $\kappa \approx \pi/2$ and $\alpha \approx 1.24$ approximate well all

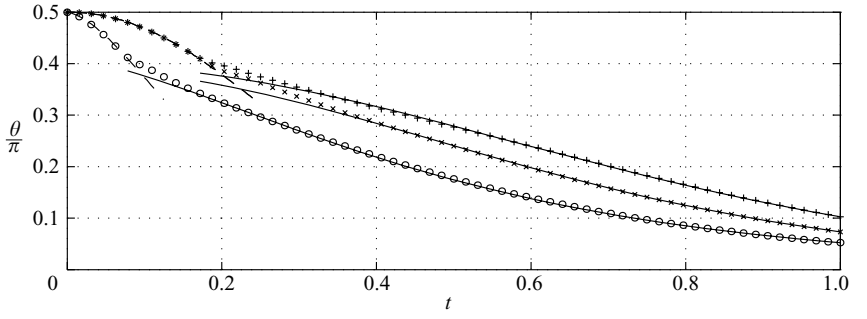

FIGURE 7. Comparison between θ computed and obtained with (4.4), dashed lines, and with (4.6), continuous lines. Case 4 ($\circ$), case 5 ($\times$), case 5 ($+$) with $Re = 2000$.

the cases with $Re = 1000$; other simulations at $Re = 2000$ give $\kappa \approx 1$ and $\alpha \approx 1.1$ in agreement with the weak Reynolds number dependence, at least for the analysed cases. The quality of the self-similar behaviour has been verified in terms of $\theta(t)$ by backward time integration of (4.6) using the known final value $\theta(1)$ as a starting condition. Illustrative results are reported in figure 7, showing that the eventual asymptotic profile is represented well by the self-similar behaviour, and that the second phase represents a rapid transition between the *no-shedding* and the *vortex-sheet* regimes.

5. Conclusions

The flow-driven opening of a rectilinear rigid inertialess leaflet in a two-dimensional channel has been studied via numerical solution of the governing equations. The standard numerical technique has been completed by a (ω, ψ) version of the immersed elements method in combination with a fluid–structure coupling technique.

The results have shown that the valve opening follows a sequence of three phases associated with specific fluid dynamics phenomena. In a first stage, the valve opens quickly without significant shedding. The leaflet motion is driven by mass conservation that, when associated with the Kutta condition at the trailing edge, gives predictable initial dynamics. During the second short phase the leaflet undergoes a significant deceleration; the formation, growth, and ejection of a primary vortex from the trailing valvular edge are the dominant features during this period. The timing of vortex shedding events can be described in terms of a modified formation time, previously introduced in different contexts (Gharib *et al.* 1998; Dabiri & Gharib 2005) that appears to properly address the vortex saturation phenomenon in this case, too. On the other hand the concept of formation time cannot be used to predict the leaflet dynamics because, in its direct evaluation form, it depends implicitly on the solution itself. The final phase is associated with the presence of a stable vortex-sheet wake and slow leaflet motion. The functional relation between valvular dynamics and fluid parameters is identified by dimensional arguments, tending asymptotically to be self-similar.

The coupled fluid–solid interaction is a central issue in several problems; it is typical in the flow crossing cardiac valves, the complete modeling of which still represents a prohibitive task, primarily because of the difficulty in collecting data about the characteristics of the solid. These obstacles can be partially overcome by developing models with potential predictive capability, in some asymptotic or approximate limit,

avoiding the need to describe material properties that are typically unavailable in biological applications. The ideal model employed here, with rigid fixed boundaries, unlimited domain, and symmetric two-dimensional flow, represents a first contribution along these lines, although the results should not be applied as such to any realistic physiological valve.

The valvular opening is found to be described by an initial no-shedding concept that jumps, through a very rapid intermediate phase, to an asymptotic self-similar behaviour, which appears consistent with varying the flow parameters. The understanding of these regimes is a preliminary starting point for the critical interpretation of results, or, for methodological extensions, for the more complex problems of three-dimensional flow through cardiac valves.

The work has been partially supported by Italian MIUR under the grant No. PRIN 2004089599.

REFERENCES

Baccani, B., Domenichini, F. & Pedrizzetti, G. 2003 Model and influence of mitral valve opening during the left ventricular filling. *J. Biomech.* **36**(3), 355–361.

Dabiri, J. O. & Gharib, M. 2005 Starting flow through nozzles with temporally variable exit diameter. *J. Fluid Mech.* **538**, 111–136.

De Hart, J., Peters, G. W. M., Schreurs, P. J. G. & Baaijens. F. P. T. 2003 A three-dimensional computational analysis of fluid-structure interaction in the aortic valve. *J. Biomech.* **36**(1), 103–112.

Domenichini, F., Pedrizzetti, G. & Baccani, B. 2005 Three-dimensional filling flow into a model left ventricle. *J. Fluid Mech.* **539**, 179–198.

Fadlun, E. A., Verzicco, R., Orlandi, P. & Mohd-Yusof, J. 2000 Combined immersed-boundary finite-difference methods for three-dimensional complex flow simulations. *J. Comput. Phys.* **161**(1), 35–60.

Gharib, M., Rambod, E. & Shariff, K. 1998 A universal time scale for vortex ring formation. *J. Fluid Mech.* **360**, 121–140.

Handke, M., Heinrichs, G., Beyersdorf, F., Olschewski, M., Bode, C. & Geibel, A. 2003 *In vivo* analysis of aortic valve dynamics by transesophageal 3-dimensional echocardiography with high temporal resolution. *J. Thorac. Cardiovasc. Surg.* **125**, 14121419.

Lemmon, J. D. & Yoganathan, A. P. 2000 Three-dimensional computational model of left heart diastolic function with Fluid-structure interaction. *J. Biomech. Engng* **122**, 109117.

Pedrizzetti, G. 1998 Fluid flow in a tube with an elastic membrane insertion. *J. Fluid Mech.* **375**, 39–64.

Pedrizzetti, G. 2005 Kinematic characterization of valvular opening. *Phys. Rev. Lett.* **94**, 194502.

Pedrizzetti, G. & Domenichini, F. 1997 Impulsive and pressure-driven transient flows in closed ducts. *Phys. Fluids.* **9**(11), 3575–3577.

Peskin, J. & McQueen D. M. 1989 A three-dimensional computational method for blood flow in the heart I. Immersed elastic fibers in a viscous incompressible fluid. *J. Comput. Phys.* **81**, 372–405.

Roache, P. J. 1998 *Fundamentals of Computational Fluid Mechanics.* Hermosa.

Stevens, C., Remme, E., LeGrice, I. & Hunter, P. 2003 Ventricular mechanics in diastole: material parameter sensitivity. *J. Biomech.* **36**(5), 737–748.

Stijnen, J. M. A., De Hart, J., Bovendeerd, P. H. M. & van de Vosse, F. N. 2004 Evaluation of a fictitious domain method for predicting dynamic response of mechanical heart valves. *J. Fluids Struct.* **19**, 835–850.

Szabo, G., Soans, D., Graf, A., Beller, C., Waite, L. & Hagl, S. 2004 A new computer model of mitral valve hemodynamics during ventricular filling. *Eur. J. Cardiothoracic Surgery* **26**, 239247.